Confinement of InO_3, InO_6, and $InBO_3$ clusters in a glass matrix

Giuseppe Faraci, Agata R. Pennisi, and Rosaria Puglisi
Dipartimento di Fisica e Astronomia, Universitá di Catania, Istituto Nazionale di Fisica della Materia, Corso Italia 57, 95129 Catania, Italy

Antonella Balerna
Istituto Nazionale di Fisica Nucleare, Laboratori Nazionali di Frascati, 00044 Frascati, Italy

Ivano Pollini
Dipartimento di Fisica, Universitá di Milano, Istituto Nazionale di Fisica della Materia, Via Celoria 16, 20133 Milano, Italy
(Received 18 September 2001; published 3 December 2001)

We report on the formation and detection of molecular aggregates of InO_x ($x=3,6$) in a glass matrix. This result was achieved by simple melting of In_2O_3 in a B_2O_3 matrix, at dilution 0.05%. At higher concentrations, we have been able to confine clusters of the mixed compound $InBO_3$, obtaining quantum dots of the indium borate embedded in the substrate. The average size of these agglomerates, evaluated in about 30 Å , does not change, increasing the dilution in the range 0.3–2.0 %. These results are of particular importance for the confinement of quantum dots in a glass matrix. The characterization of the samples was performed by extended x-ray-absorpion fine-structure and x-ray-diffraction spectroscopies.

DOI: 10.1103/PhysRevB.65.024101 PACS number(s): 61.46.+w, 61.10.Ht, 61.10.−i

I. INTRODUCTION

The optical properties of luminescent oxides are widely studied; doped or undoped glasses, such as orthoborate compounds, [1–3] represent an interesting class of materials, which can exhibit high optical trasparency and/or good electrical conductivity. A similar behavior can be found in metal oxides,[4–8] such as In_2O_3 or SnO_2, which are considered to be high-gap semiconductors. These materials also find technological application in heterojunctions, solar cells, and microdevices. An interesting compound is represented by indium borate ($InBO_3$),[9] where the trivalent atoms can be easily substituted for by other impurities for a proper doping of the pure crystal, obtaining promising applications.[10] The bulk or thin-film properties of these oxides can be dramatically improved when the material is confined in a matrix in the nanometer range, since quantum size effects modify the relative energy levels. To this end quantum wells, and in particular zero-dimension nanocrystals (quantum dots), have been widely studied and realized mainly for laser applications and similar optoelectronic devices.[11,12] Of our present studies on cluster confinement,[13–15] here we investigate the growth mechanism of $InBO_3$ nanocrystals in a glass matrix, and in particular the cluster size and size distribution, the stoichiometry, and the structure inside and at the interface of the quantum dot. Indeed, the characteristics of the nanoparticles, i.e., the structural, optical, and electrical properties, strongly depend on the growth details including the thermal treatment.

In order to obtain size-selected quantum dots, different procedures have been adopted; one of the most suitable is the three-dimensional clustering from a solid solution in a glass.[16] As our study concerns the growth of size-selected $InBO_3$ clusters, it is obvious to choose a B_2O_3 oxide as the glass matrix. In fact this matrix is an insulating crystalline material which undergoes undercooled melt in a wide temperature range that can be modified by addition of convenient impurities; in this range the diffusion of a diluted solute can be controlled just modifying the viscosity of the matrix. The melting point $T_m(B_2O_3)$ is 723 K, and the corresponding glass transition range is $T_g=470–530$ K, but the viscosity changes as a function of the temperature and of the doping; therefore, the heat treatment can be set over a wide range depending on the composition.

On the other hand, x-ray-diffraction measurements and optical spectra [1] for doped $InBO_3$ showed a wide morphology with a glass transition temperature at 506 °C and a crystallization temperature at 740 ° C; therefore, we can use the entire glass transition range for the controlled precipitation of quantum dots as nanocrystalline clusters.

In order to determine the local configuration, i.e., if the clusters are in a crystalline phase, the nearest-neighbor distance, the relative coordination number, and similar information for some successive shells, we used the Extended X-ray Absorption Fine Structure (EXAFS) spectroscopy available at the European Synchrotron Radiation Facility (ESRF, Grenoble, France). In fact, this technique allows an investigation of the geometrical configuration around the absorbing In atom, permitting one to distinguish between oxygen, boron, and indium coordinations; moreover, it is possible to determine the mutual distance related to the eventual distortion of the lattice, i.e., to compression (or expansion) strain induced in the clusters; finally, another important piece of information obtained by these measurements is the vibrational and thermodynamical parameters (Debye-Waller factor and Debye temperature), and the interface configuration related to the phonon coupling with the matrix.[13–15] The EXAFS measurements were corroborated by conventional XRD (x-ray-diffraction) spectra both for diluted samples and for the reference compounds.

In the present study we report on an investigation of the structural and dynamical properties of $InBO_3$ nanoclusters

TABLE I. Reference crystalline In_2O_3, and $InBO_3$ 5.0%. First, second, third, and fourth shells around an In absorber obtained by the standard diffraction analysis and by the FEFFIT code applied to FT's of the EXAFS spectra; here the uncertainty for all the coordination numbers is ± 0.1, that for the fitted distances is ± 0.01 Å, and that for the DW factors is ± 0.0002 Å^2.

			Diffraction		EXAFS		
Crystal	Coordination	Bond	N	R (Å)	N	R(Å)	$\sigma^2(\times 10^{-4}$ Å$^2)$
In_2O_3							
	I	In-O	6.0	2.1706	6.0	2.17	39.0
	II	In-In	6.0	3.3601	6.0	3.35	21.0
	III	In-In	6.0	3.8085	6.0	3.83	28.0
	IV	In-O	6.0	4.0094	6.0	4.01	38.0
$InBO_3$							
	I	In-O	6.0	2.1576	6.0	2.157	26.0
	II	In-B	6.0	3.0667	6.0	3.07	26.0
	III	In-O	6.0	3.3629	6.0	3.37	16.0
	IV	In-In	6.0	3.7908	6.0	3.79	25.0

confined in the matrix for samples in very diluted regime, up to 5.0%. At very low dilution, it was possible to confine in the matrix single InO_3 and InO_6 molecules, whereas clusters of $InBO_3$ were detected in the range 0.1–2.0 %.

II. EXPERIMENT

The synthesis of $InBO_3$ clusters was obtained from high-purity constituents (In_2O_3, indium oxide, and B_2O_3, boron oxide) by controlled melting under an argon atmosphere; our procedure was rather simpler than the one reported in Refs. 1 and 9; we carefully mixed the constituents at the proper concentration, warming up to 1000 °C for about 30 m, and slowly cooling down to room temperature afterwards.[16]

Care was taken to obtain only agglomerates of a single compound in the matrix, in the present case $InBO_3$ without any precipitate of indium oxide; this is possible in the initial indium oxide solute by substituting a trivalent indium atom with a still trivalent boron atom in the chemical formula. A different method should be adopted in order to confine In_2O_3 clusters in the boron oxide matrix; this will be the subject of a forthcoming paper. As shown below, the measurements allowed us to check the composition of each sample, and no simultaneous presence of the two compounds was detected. We point out, first, the different composition and geometrical configuration of the constituents, which should be recalled before discussing our results. The bulk crystal structure of an In_2O_3 sesquioxide is the cubic bixbyite[17] configuration described as an incomplete cubic close packing of oxygen ions around the metal; here six oxygen atoms are around a central In absorber, at 2.17 Å. Second and third coordination shells, of six In atoms each, surround the central In at 3.36 and 3.80 Å; the fourth and fifth shells are constituted by 6+6 oxygen atoms at 4.01 and 4.12 Å, respectively. Higher In shells are at 5.06 and 6.07 Å. In contrast, the crystalline configuration of the $InBO_3$ oxide, recently determined by Cox and Keszler,[9] is formed by layers of distorted InO_6 octahedra, connected to triangular-planar BO_3 units. The crystal structure is rhombohedral with hexagonal axes $a=4.8217$ Å and $c=15.438$ Å, where In is at the origin (0,0,0), oxygen at (0.7138, 0, 0.25) and boron at (0, 0, 0.25). The coordination numbers and distances easily obtained from the crystal structure are displayed in Table I. We point out that, although the first coordination around In is in any case due to six oxygen atoms, the configuration is quite different between indium oxide and indium borate; in fact, not only is the first distance In-O different between the two oxides, but in addition the angle O-In-O changes from 91.9° in the indium borate to 79.3° in the indium oxide.

The EXAFS experiment was performed at the GILDA beamline of ESRF; the radiation was monochromatized and horizontally focused by a crystal Si(311) monochromator. The beam spot on the sample was 1×2 mm^2; the energy resolution was of the order of 10^{-5}. X-ray spectra were collected around the In K edge (27940 eV). The measurements were performed at 77 K, in fluorescence using an ultrapure 13-element Ge multidetector cooled at 77 K; however, the absorption detection was adopted for high concentration (0.4–5.0 %) samples, considering the very low absorbance of the matrix. For reference, a high-purity In foil was used, together with a thin layer of In_2O_3 powder polycrystal, and an $InBO_3$ 5% solid solution. In addition, conventional x-ray-diffraction spectra were also collected on each sample, in order to test not only the reference materials but also the thin layers synthesized at several dilution percentages. The normalized EXAFS spectra were analyzed according to a standard procedure,[18,19] removing the background by means of a cubic spline and fitting the continuous component of the spectrum in the k range. From the raw curves, after normalization and subtraction of the background, we can extract the EXAFS oscillations $\chi(k)$. These curves, weighted by k^2 or k^3, have been Fourier transformed in the range $\Delta k = 3.2$–16.5 Å^{-1}. Their peaks correspond to the first coordination shell and successive coordination shells due to the local average configuration of each sample.

First of all, in Fig. 1 we show the EXAFS oscillations $\chi(k)$ for the two reference thin layers In_2O_3 and $InBO_3$ 5%; in Fig. 2, the Fourier transforms (FT) of the $\chi(k)$ weighted

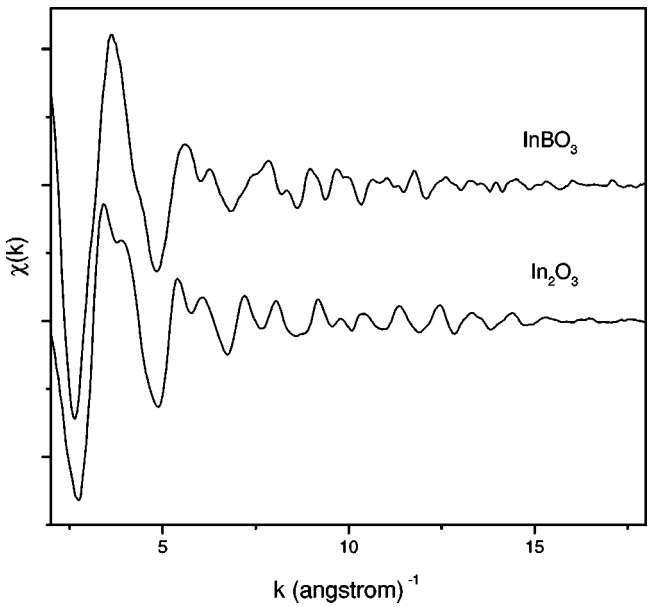

FIG. 1. EXAFS oscillations of the reference samples, as a function of the wave vector *k*, extracted from the raw spectra after normalization and background subtraction. For the sake of clarity, the curves were shifted in the vertical direction.

by k^3 are included; note that the long range of the *k* spectra optimizes the resolution of the Fourier transforms, allowing the separation of adjacent features; these correspond in real space to first, second, and successive coordination shells around the In absorber. To fully individuate the parameters of

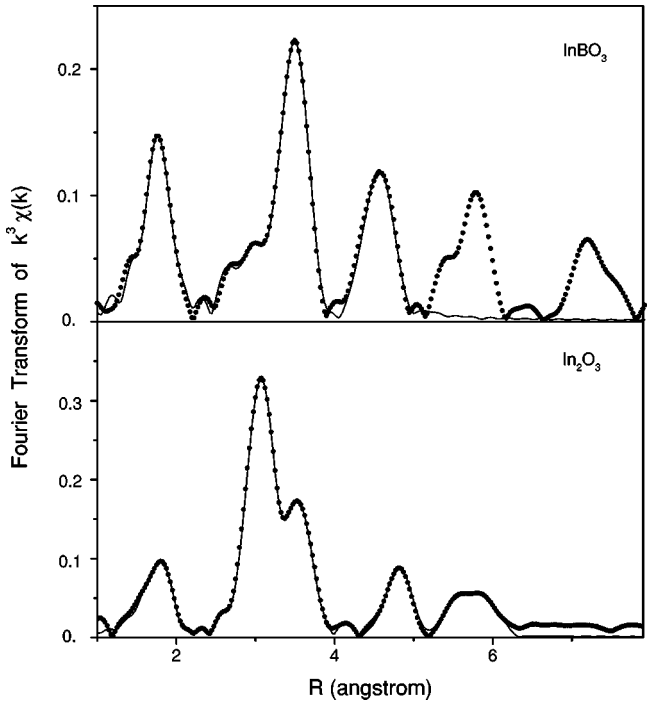

FIG. 2. Reference samples. Fourier transforms (dotted line) of k^3 weighted $\chi(k)$, together with the fitting curves (continuous line) obtained using the FEFFIT code. The parameters obtained by this procedure are reported in Table I.

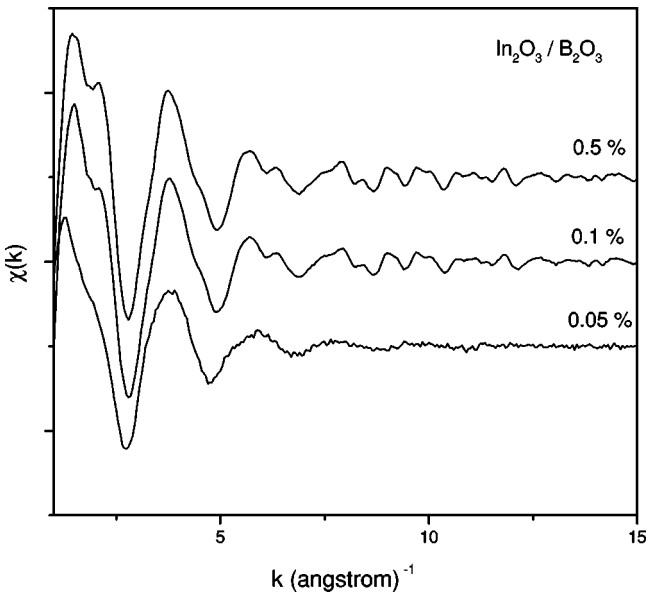

FIG. 3. Typical diluted samples: EXAFS oscillations, as a function of the wave vector *k*, extracted from the raw spectra after normalization and background subtraction. For the sake of clarity, the curves were shifted in the vertical direction. Also note the XANES (near-edge) region.

each shell in the FT, we used an accurate fitting procedure[20,21] on the EXAFS signal and on the Fourier transforms, which includes curved wave effects, multiple-scattering paths, and inelastic losses. This fit gives the best values for the parameters involved in this spectroscopic technique, i.e., the coordination number *N*, the relative distance *R*, and the Debye-Waller (DW) factor σ for each shell. In order to compare the relative differences between the two oxides, we used the previous structures for our reference samples, obtaining the best fits of the parameters characterizing each shell; these plots are reported in Fig. 2, and the fitted parameters are included in Table I; an excellent agreement is evident with the geometrical data of the literature. In addition, the fits allowed a determination of the DW factor, denoting the mean-squared relative atomic displacement for each shell, also report in Table I.

After a careful check of the reference compounds, we can present the measurements performed on our samples for dilutions of 0.1–0.5 %, 2.0%, and about 0.05%. This last concentration is uncertain by 50%, the others by less than 10%. The homogeneity of the samples was tested by collecting spectra on different spots of the sample: no detectable difference was found by modifying the position of the beam on the sample. In Fig. 3, the EXAFS spectra for our samples are reported. Looking at this figure, we observe a dramatic difference between the lowest dilution spectrum and all the others; in fact the 0.05% curve presents only a main frequency, whereas the others look very similar and show several overlapping components. In fact, the Fourier transforms presented in Fig. 4, and compared to the reference compounds, confirm this.

(i) Only a single coordination shell is present at the lowest dilution, corresponding to an In-O first peak at 2.09 ± 0.01 Å

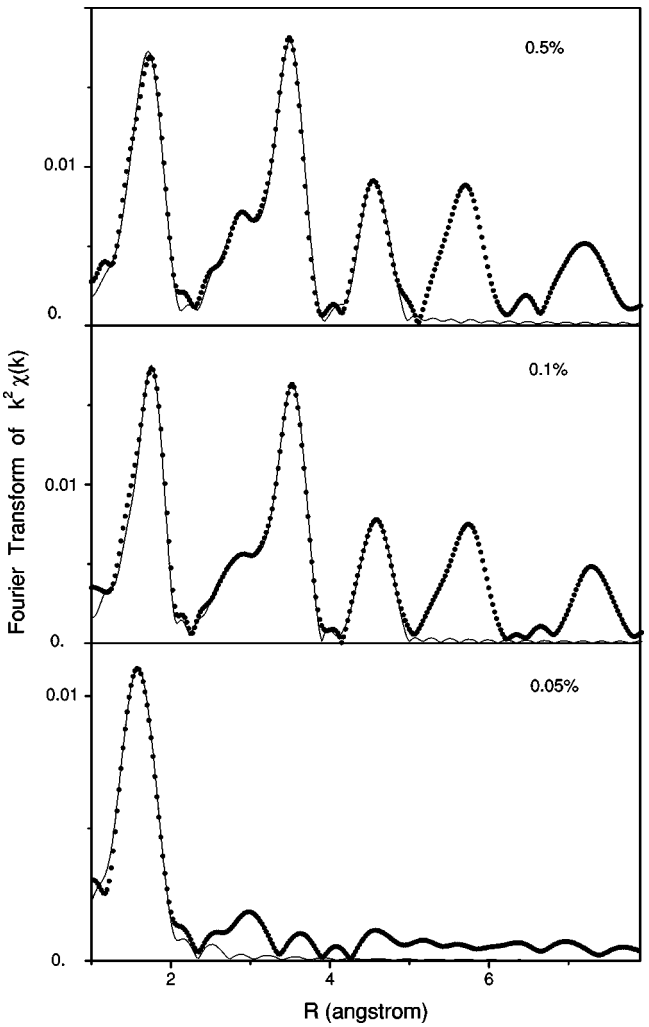

FIG. 4. Fourier transforms (dotted line) of k^2 weighted $\chi(k)$, together with the fitting curves (continuous line) obtained using the FEFFIT code, for the same samples as in the previous figure. The parameters obtained by this procedure are reported in Table II. The main peak is due to the oxygen coordination shell around the In absorber. No other features is clearly visible out of the noise level at the lowest dilution. The other spectra present the same peaks due to the second, third, and fourth shells. Also visible are two other features arising mainly from higher metal shells which were not fitted.

contracted with respect to the crystal by 0.067 Å ; no other feature is clearly visible, denoting the presence of small molecules where In is bound to oxygen in an ordered configuration. The fit of the coordination number and of the DW factor gives a reduced coordination of 5.0 ± 0.2, with a $\sigma^2 = 0.0022$ Å ^{2}. Taking into account the strong asymmetry of this oxygen shell, we carried out a more detailed analysis introducing the fourth cumulant in the fit; as is well known, this parameter provides information about the shape of the peak[22–24]; actually, we obtained a value for this cumulant $C_4 = 1.9\times10^{-5}$ Å ^{4}, indicating, as expected, that the oxygen environment is strongly distorted.

The strong modification of the EXAFS curve and of the corresponding FT, appearing for this sample at the lowest concentration, can also be observed in the raw absorption curves, just after the threshold, around the XANES (x-ray-absorption near-edge spectrum) region (Fig. 3); in fact, after the main peak a feature at 0.1% and 0.5%, missing at the lowest dilution, is visible; in addition, the following oscillations display additional structures absent at 0.05%. This is a clear symptom of a different chemical environment around the metal absorber with a modified local configuration.

(ii) In contrast to the very diluted concentration, samples at any other percentage are very close to the $InBO_3$ crystalline solid solution, and present (see Fig. 4) all the peaks corresponding to several coordination shells, whose parameters are fully reported in Table II. Here too, the fourth cumulant for the first shell was fitted with a value $C_4 = -1.0\times10^{-5}$ Å ^{4}. No correlation of this cumulant was observed with the other three parameters of the same shell. Also note the different asymmetry with respect to the value obtained at 0.05%.

III. DISCUSSION

In contrast with the reference, as already emphasized, for the diluted sample (0.05%) as a consequence of the dilution process, in the FT (see Fig. 4) we only obtain the first peak, which should be ascribed to nearest neighbors of the In central atom; this peak is therefore due to oxygen. However, we observe a coordination number limited to only five oxygen atoms, i.e., a ''molecular distribution'' of InO_x *molecules* confined in the matrix, with an average coordination reduced

TABLE II. First, second, third, and fourth shells around an In absorber for our diluted samples, obtained by the FEFFIT code applied to FT's of the EXAFS spectra; here the uncertainty for the coordination numbers is ±0.1, and that for the lowest dilution ±0.2; for all fitted distances the uncertainty is ±0.01 Å , that for the DW factors of the first and last shells is ±0.0002 Å ^{2}, and that for the second and third shells is ±0.0008 Å ^{2}.

	First shell: In-O			Second shell:In-B			Third shell:In-O			Fourth shell:In-In		
Dilution (%)	N	R (Å)	$\sigma^2(\times10^{-4}$ Å $^2)$	N	R (Å)	$\sigma^2(\times10^{-4}$ Å $^2)$	N	R (Å)	$\sigma^2(\times10^{-4}$ Å $^2)$	N	R (Å)	$\sigma^2(\times10^{-4}$ Å $^2)$
0.05	5.0	2.09	22.0	–	–	–	–	–	–	–	–	–
0.1	6.0	2.151	33.0	5.9	3.07	40.0	5.9	3.37	36.0	5.2	3.80	25.0
0.2	6.0	2.154	38.0	6.0	3.06	41.0	6.0	3.37	26.0	5.5	3.79	25.0
0.3	6.0	2.153	31.0	6.0	3.06	23.0	6.0	3.37	29.0	5.4	3.79	21.0
0.5	6.0	2.151	27.0	5.9	3.05	40.0	6.0	3.34	17.0	5.5	3.79	26.0
2.0	6.0	2.154	31.0	6.0	3.07	46.0	6.0	3.34	17.0	5.4	3.80	26.0
5.0	6.0	2.157	26.0	6.0	3.07	26.0	6.0	3.37	16.0	6.0	3.79	25.0

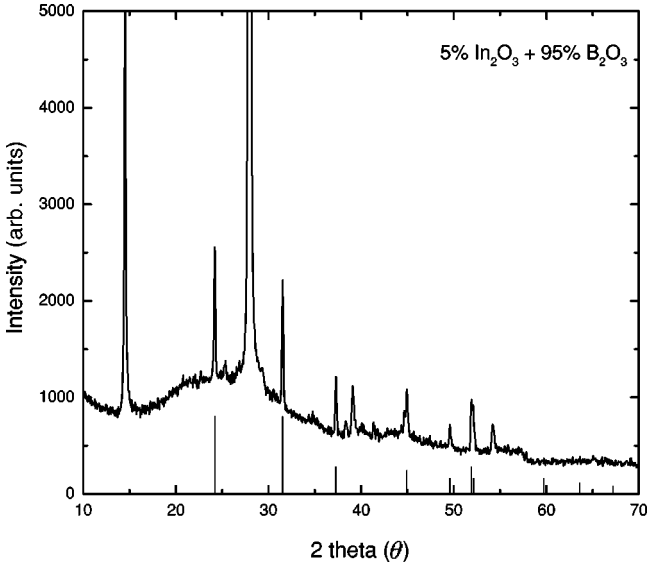

FIG. 5. Diffraction spectrum for the sample at 5% dilution. The peaks indicated by the bottom lines are due to $InBO_3$ crystalline precipitates. The highest peaks are due to the boron oxide matrix.

to five nearest neighbors; no evidence is found of second or higher shells, as can be seen in the flat high tail of the FT . We point out the following interesting results (see Table II): (i) an average coordination number, limited to only 5 instead of 6, can be simply attributed to the presence of InO_3 and InO_6 aggregates roughly with relative percentages of 70% and 30%. This interpretation would imply that at the lowest concentration the bonds of the InO_6 octahedra between the aggregates or with BO_3 units are broken or at least very disordered. However, the confinement of single InO_3 ''molecules'' in the matrix can be due to a metal atom bound in a substoichiometric oxidation state with oxygen; the three oxygen atoms in turn might be bound to another oxygen or boron atom of the matrix, but without any ordered configuration. This could be an early stage of the breaking of the solute In_2O_3 in its small base entities, before the indium borate clusters precipitate.

The previous conclusion also excludes any possible amorphization of the sample at least at short range; in fact, an amorphization would imply the full coordination of the first shell around In, and we should find six oxygen atoms in first shell. This is not the case. We can also exclude the amorphization of the matrix: in fact, the XRD pattern of these samples shows all the diffraction peaks of the pure B_2O_3 (see Fig. 5).

Furthermore, the presence of both InO_6 and InO_3 clusters excludes the formation of any aggregate of In_2O_3; in this case, in fact, we should find six oxygen atoms in the first shell, and second and third shells of In atoms, as in the corresponding reference sample. Of course, the size of the agglomerates (and their size distribution, which is averaged over) could produce a reduction of the second and third coordination numbers, since the cluster surface, interfaced to the glass matrix, contributes less than the internal In atoms, at least as far as the metal coordination is concerned. Therefore, at low concentrations, the formation of nanoclusters of either a solute or a mixed compound can also be excluded, considering the absence of second and third shells of either indium, boron, or oxygen.

At present, we attribute the molecular confinement to the strength of the metal-oxygen bonds, which are much stronger than the metal-metal interaction. Taking into account the electron negativity of In (1.7) with respect to that of oxygen (3.5), it is very likely that the trivalent In metal binds to three or six oxygen atoms in a partially covalent configuration. Also note the contracted distance In-O for these molecules and the somewhat reduced Debye-Waller factor. These characteristics should be attributed to the modified environment around the metal absorber.

Looking now at Figs. 3 and 4, we observe that samples at 0.1–0.5 % present very similar EXAFS curves, demonstrating that the dilution process has produced, already at 0.1%, a precipitation of small $InBO_3$ clusters, since the entire sequence of the indium coordination shells is very comparable to the indium borate reference. In fact, the fitting analysis (see the corresponding parameters reported in Table II), confirms the presence of a first shell of six oxygen atoms around the absorber at 2.15 Å ; furthermore, the successive shells are quite evident: in fact, after the first peak due to oxygen, we find evidence of a second boron shell, of a third oxygen shell, and of a fourth indium shell. This last has a somewhat reduced coordination with respect to the crystalline $InBO_3$. Also quite clear are other, higher, shells where contributions from oxygen shells and metal shells overlap together with several multiple-scattering contributions due to three or more paths.[20,21] For this reason we did not attempt to disentangle these features even though the metal backscattering amplitude widely overwhelms the oxygen amplitude.

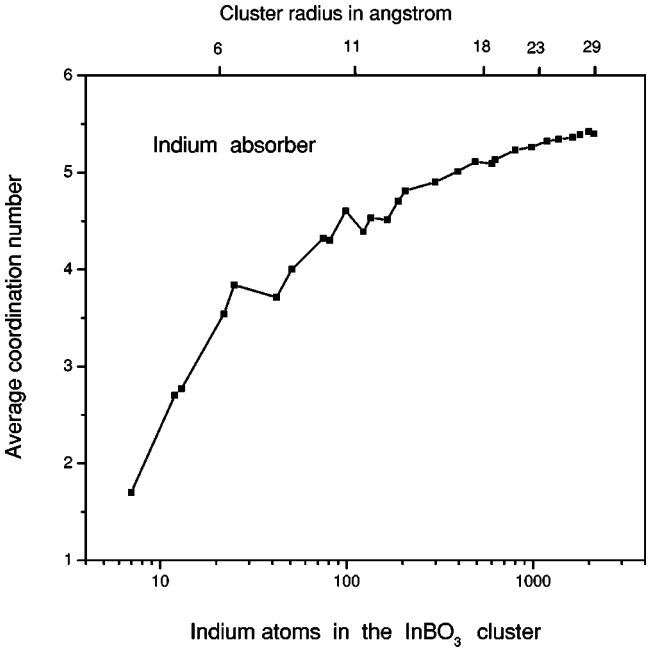

FIG. 6. Average coordination In-In for $InBO_3$ clusters as a function of the size. The reduction with respect to the bulk value is due to the surface contribution. The continuous line is a guide to the eye.

It is also worth noting that the fitted coordination number of In-In is somewhat reduced, denoting a limited size nanoaggregate; this effect is clearly ascribed to the surface configuration, which contributes dramatically less than the internal part of the cluster, as concerns the In-In coordination. Conversely, the oxygen coordination is not modified at all, and this confirms that these agglomerates always have a complete oxygen shell at their interface with the matrix.

Furthermore, considering the very close values of the parameters obtained for dilutions differing by a factor of 20, we argue that the size of the clusters distributed in the matrix does not increase with the percentage of solute, but very likely reaches a constant value at least in this range of concentration. This is a crucial point for producing a size-selected quantum dot ensemble.

The results presented above demonstrate the possibility of a confinement of clusters of indium borate caused by simple melting at low concentration of indium oxide in boron oxide. In order to determine the size of the clusters, it is enough to calculate the average coordination around the central metal atom as a function of the radius of the cluster. Using the crystal configuration, we evaluate that, in a sphere of 12-Å radius, there are 135 In (or B) and 410 O atoms around the absorber: for such a cluster the In-O average first coordination is 5.15, the second shell (In-B) has a coordination of 4.93, the third shell (In-O) one of 4.84 and the fourth (In-In) one of 4.53. A plot of the modification of the average coordination as a function of the size of the cluster[22–24] is reported in Fig. 6. With the experimental values given in Table I, we therefore calculated the radius of the clusters to be about 30 Å , where about 2000 indium atoms and 2000 boron atoms reside. In conclusion, the confinement of quantum dots was clearly demonstrated in a set of samples, since the coordination number of In-In does not change although the concentration increases by an order of magnitude. We have obtained a result concerning the uniform confinement of molecular InO_3 and InO_6 clusters, using a low dilution of indium oxide in a glass matrix, and a result concerning the confinement of larger $InBO_3$ quantum dots of 30-Å radius, in a range of dilution where the average size of these clusters remains quite stable.

ACKNOWLEDGMENTS

We wish to acknowledge the staff of GILDA and ESRF for the excellent assistance during the experiments. Thanks are due in particular to Stefano Colonna and Pierlorenzo Solari of the GILDA beamline, and to G. Malandrino for the diffraction analyses. We thank also D. Cipriani for the sample preparation.

[1] K. Tanaka, N. Tamura, K. Hirao, and N. Soga, Mater. Chem. Phys. **59**, 82 (1999).
[2] G. Blasse, C. De Mello Donegá, N. Efryushina, V. Dotsenko, and I. Berezovskaya, Solid State Commun. **92**, 687 (1994).
[3] V. Dotsenko, N. Efryushina, and A. Nazarenko, Opt. Spectrosc. **69**, 622 (1990).
[4] G. Golan, A. Axelevitch, and E. Rabinovitch, J. Vac. Sci. Technol. A **16**, 2614 (1998); F. O. Adurodija, H. Izumi, T. Ishihara, H. Yoshioka, H. Matsui, and M. Motoyama, Appl. Phys. Lett. **74**, 3059 (1999).
[5] R. B. H. Tahar, T. Ban, Y. Ohya, and Y. Takahashi, J. Appl. Phys. **82**, 865 (1997).
[6] S. Dakshina Murthy, E. Langlois, I. Bhat, R. Gutmann, E. Brown, R. Dzeindziel, M. Freeman, and N. Choudhury, in *The Second NREL Conference on Thermophotovoltaic Generation of Electricity*, edited by John P. Benner, Timothy J. Coutts, and David S. Ginely, AIP Conf. Proc. No. 358 (AIP, Woodbury, NY, 1996), p. 290.
[7] C. Xirouchaki, G. Kiriakidis, T. F. Pedersen, and H. Fritzsche, J. Appl. Phys. **79**, 9349 (1996).
[8] M. Mizuno, T. Miyamoto, T. Ohnishi, and H. Hayashi, Jpn. J. Appl. Phys. **36**, 3408 (1997); H. Kim, C. M. Gilmore, A. Piqué, J. S. Ilorwitz, H. Mattoussi, H. Murata, Z. H. Kafafi, and D. B. Chrisey, J. Appl. Phys. **86**, 6451 (1999).
[9] J. R. Cox and D. A. Keszler, Acta Crystallogr., Sect. C: Cryst. Struct. Commun. **50**, 1857 (1994).
[10] T. Welker, J. Lumin. **48/49**, 49 (1991).
[11] H. Zhou, W. Cai, and L. Zhang, Appl. Phys. Lett. **75**, 495 (1999).
[12] N. N. Ledentsov, Semiconductors **33**, 946 (1999), and references therein.
[13] G. Faraci, A. R. Pennisi, A. Balerna, H. Pattyn, G. E. J. Koops, and G. Zhang, Phys. Rev. Lett. **86**, 3566 (2001); G. Faraci, S. La Rosa, A. R. Pennisi, S. Mobilio, and G. Tourillon, Phys. Rev. B **43**, 9962 (1991).
[14] A. Pinto, A. R. Pennisi, G. Faraci, G. D'Agostino, S. Mobilio, and F. Boscherini, Phys. Rev. B **51**, 5315 (1995); G. Faraci, S. La Rosa, A. R. Pennisi, S. Mobilio, and I. Pollini, *ibid.* **45**, 9357 (1992).
[15] G. Faraci, A. R. Pennisi, and J. L. Hazemann, Phys. Rev. B **56**, 12 553 (1997); F. Zontone, F. D'Acapito, G. Faraci, and A. R. Pennisi, Eur. Phys. J. B **19**, 501 (2001).
[16] U. Woggon, *Optical Properties of Semiconductor Quantum Dots* (Springer-Verlag, Berlin, 1997).
[17] R. W. G. Wyckoff, *Crystal Structures* (Wiley, New York, 1964).
[18] P. A. Lee, P. H. Citrin, P. Eisenberger, and B. M. Kincaid, Rev. Mod. Phys. **53**, 769 (1981).
[19] E. A. Stern, B. A. Bunker, and S. M. Heald, Phys. Rev. B **21**, 5521 (1980).
[20] J. Mustre de Leon, J. J. Rehr, S. I. Zabinsky, and R. C. Alberts, Phys. Rev. B **44**, 4146 (1991); J. J. Rehr, R. C. Alberts, and S. I. Zabinsky, Phys. Rev. Lett. **69**, 3397 (1992).
[21] J. J. Rehr, S. I. Zabinsky, A. Ankudinov, and R. C. Alberts, Physica B **208-209**, 23 (1995); E. A. Stern, M. Newville, B. Ravel, Y. Yacoby, *ibid.* **208-209**, 117 (1995).
[22] P. A. Montano, G. K. Shenoy, E. E. Alp, W. Schulze, and J. Urban, Phys. Rev. Lett. **56**, 2076 (1986).
[23] P. A. Montano, W. Schulze, B. Tesche, G. K. Shenoy, and T. I. Morrison, Phys. Rev. B **30**, 672 (1984).
[24] M. A. Marcus, M. P. Andrews, J. Zegenhagen, A. S. Bommannavar, and P. Montano, Phys. Rev. B **42**, 3312 (1990).